Lamin B1 regulates somatic mutation and progression of B cell malignancies

Running title: Lamin B1 inhibits somatic mutations

Tetyana Klymenko[1*%], Johannes Bloehdorn[2*], Jasmin Bahlo[3], Sandra Robrecht[3], Andrew Clear[1], Kerry Cox[4], Sven Estenfelder[2], Jun Wang[1], Jennifer Edelmann[1], Jonathan C. Strefford[4], Tomasz K. Wojdacz[4,5], Kirsten Fischer[3], Michael Hallek[3], Stephan Stilgenbauer[2], Mark Cragg[4], John Gribben[1], Andrejs Braun[1].

[1]Centre for Haemato-oncology, Barts Cancer Institute, Queen Mary University, London, United Kingdom.

[2]Department of Internal Medicine III, University of Ulm, Ulm, Germany.

[3]Department I of Internal Medicine, Center for Integrated Oncology Cologne, University Hospital of Cologne, Cologne, Germany.

[4]Academic Unit of Cancer Sciences, Faculty of Medicine, Cancer Research UK Centre and Experimental Cancer Medicine Centre, University of Southampton, Southampton, UK.

[5]Aarhus Institute of Advanced Studies, Aarhus University, Aarhus, Denmark.

[*]These authors contributed equally to this work and therefore should be considered as joint first authors.

[%]Current address: Biomedical Research Centre, Sheffield Hallam University, City Campus, Sheffield S1 1WB, UK.

Correspondence should be addressed to: Andrejs Braun, Barts Cancer Institute, Queen Mary University of London, John Vane Science Centre, Charterhouse Square, London EC1M 6BQ. United Kingdom. Tel: +44 (0)20 7882 3816 | Fax: +44 (0)20 7882 3816 | Email: andrejs.braun@qmul.ac.uk ; or to John Gribben Queen Mary University of London, 3rd Flr John Vane Science Centre, Charterhouse Square, London EC1M 6BQ, Tel: 020 7882 3804

Fax 020 7882 3891, email: j.gribben@qmul.ac.uk

Abstract

Somatic hypermutation (SHM) is a pivotal process in adaptive immunity that occurs in the germinal centre and allows B cells to change their primary DNA sequence and diversify their antigen receptors. Here, we report that genome binding of Lamin B1, a component of the nuclear envelope involved in epigenetic chromatin regulation, is reduced during B cell activation and formation of lymphoid germinal centres. ChIP-Seq analysis showed that kappa and heavy variable immunoglobulin domains were released from the Lamin B1 suppressive environment when SHM was induced in B cells. RNAi-mediated reduction of Lamin B1 resulted in spontaneous SHM as well as kappa-light chain aberrant surface expression. Finally, Lamin B1 expression level correlated with progression-free and overall survival in chronic lymphocytic leukaemia, and was strongly involved in the transformation of follicular lymphoma. In summary, here we report that Lamin B1 is a negative epigenetic regulator of SHM in normal B-cells and a "mutational gatekeeper", suppressing the aberrant mutations that drive lymphoid malignancy.

Introduction

Class-Switch Recombination (CSR) and somatic hypermutation (SHM) are biological mechanisms through which B cells adapt and respond to pathogens. These mechanisms involve a regulated process of targeted mutation within the variable regions of immunoglobulin genes, thus diversifying the antibody repertoire and allowing affinity maturation and isotype class switching. There is increasing evidence that epigenetic factors, such as DNA methylation and post-translational histone modifications, play major roles in regulating CSR and SHM (1). In addition to regulating expression of the central mutating enzyme activation-induced cytidine deaminase (AID), these epigenetic factors (e.g. Spt6, $H2B^{Ser14p}$) also target the SHM/CSR machinery, in a manner independent of V(D)J or S region transcription, by inducing an open chromatin state and recruiting critical adaptor proteins (2-4). Thus, B cell SHM can be regulated by a higher order of chromatin organisation.

From that perspective, it is intriguing that the subnuclear position of chromatin domains (i.e. proximity to the nuclear envelope) has been suggested to impact both transcription and V(D)J recombination (5). Furthermore, peripheral interphase relocalisation of immunoglobulin variable regions during both B cell development (5) and antibody production in plasma cells (6), suggests an “in situ” epigenetic mechanism by which sub-telomeric (IgHV) or peri-centromeric (IgKV and IgLV) immunoglobulin variable loci can transition from repressive to permissive chromatin states to facilitate rearrangement.

The nuclear periphery, containing the IgH and IgK gene clusters (5, 7), is a unique compartment comprised of inner nuclear membrane proteins and nuclear lamina (8). Previous genome-wide and cytological studies revealed the regulatory role for some of these nuclear proteins in higher level genome organisation and gene regulation (9). In particular, Lamina Associated Domains (LADs) were identified at the nuclear periphery using the DNA Adenine Methyltransferase Identification (DamID) technique (10). Initial reports described LADs as large (0.1 – 10 Mb), transcriptionally silent, gene-poor domains associated with Lamin B1, comprising of up to a quarter of nuclear chromatin (10). More recent studies have also revealed an important role of LADs in the regulation of gene expression and recombination (11, 12). Moreover, developmentally regulated genes were found to be specifically enriched in these domains (13, 14), leading to the theory that LADs are regulated as facultative heterochromatin compartments during development. In agreement with this, large-scale chromatin relaxation and aberrant transcription were specifically linked to Lamin B1 depletion in senescent fibroblasts and progeria cells (15, 16). Furthermore, age-associated loss of Lamin B1 has been reported to lead to systemic inflammation in Drosophila due to the derepression of a large number of immune responsive genes (17). These data strongly suggest the restrictive role of LADs in epigenetic gene regulation. This restrictive influence can be transient and tightly regulated depending on the cellular differentiation state.

Topologically, centromeric and telomeric chromosome regions were the primary candidates for lamina-mediated epigenetic gene regulation as both were shown to colocalise with intra-nuclear lamina structures resulting in their preferred peripheral distribution (18, 19).

Given the apparent topological coincidence between LADs and Ig variable clusters, we hypothesised that nuclear lamina might play a paramount role in the dynamics of Ig-

encoding variable genome clusters. In particular, here we tested whether Lamin B1, a principal LAD-associated component of the nuclear envelope, had any restrictive role on somatic hypermutation (SHM) and the expression of Ig genes. Due to the strong involvement of IgV mutations in the pathogenesis of B-cell malignancies, we also tested whether nuclear lamina is involved in the pathogenesis of germinal centre lymphomas and chronic lymphocytic leukaemia (CLL). Finally, we have elucidated associations of Lamin B1 expression with other prognostic factors in CLL and its impact on the disease course in a front-line clinical treatment trial (CLL8 study).

Materials and Methods

Cell lines

Pfeiffer, Raji, and SU-DHL4 cells were obtained from American Type Culture Collection (ATCC). EHEB and Karpas422 cell lines were obtained from European Collection of Authenticated Cell Cultures (ECACC, Public Health England). BL2 cell line was obtained from the German Collection of Microorganisms and Cell culture (ACC 625. Deutsche Sammlung von Mikroorganismen und Zellkulturen, DSMZ). Cells were maintained in antibiotic-free RPMI 1640 medium with FCS (10%; Sigma-Aldrich) and glutamine (2 mM; Gibco, Invitrogen) at 37°C, 5% CO2, and were routinely screened for mycoplasma contamination. Cytogenetically, BL2 cells were characterised as human flat-moded near-diploid karyotype with 3% polyploidy; 44-47<2n>XY, der(1)t(1;7)(q32;q11.2), der(6)t(1;6)(q21;q25), t(8;22)(q24;q11.2), del(11)(q24.2); carrying t(8;22) effecting juxtaposition of MYC with IGL@. Immunophenotypically, cells were CD3 -, CD10 +, CD13 -, CD19 +, CD20 +, CD34 -, CD37 +, CD38 +, cyCD79a +, CD80 +, CD138 -, HLA-DR +, sm/cyIgG -, sm/cyIgM +, sm/cy kappa -, sm/cy lambda +.

Induction and quantification of somatic hypermutation in the Ig V gene

In vitro SHM was induced as described (20) with minor modifications. Cells were incubated at $2x10^6$ cells/ml in RPMI medium, containing 2.5 μg/ml of biotinylated anti−human IgM (clone UCHB1 Caltag Laboratories, Buckingham, UK), 10ug/ml of anti-CD19 (clone RFB9, in-house, Southampton, UK) and 10ug/ml of anti-CD21 (clone HB135, in-house, Southampton, UK) for 20 min at 4 °C. Cells were washed and then resuspended in RPMI medium containing streptavidin-conjugated magnetic beads (5−7 beads/cell) (Dynabeads M280, Thermo-Fisher, UK) and incubated with agitation at 4 °C for 20 min. Complete RPMI medium containing 10% FBS was added to the activated cells to a final density of $1x10^6$, followed by incubation at 37 °C for 24h, 48h or 72h. To analyse Ig gene hypermutation, the V4-39-JH5 gene was amplified from genomic DNA with Pfu DNA polymerase (Thermo Scientific). The primers used were Vh4-forward 5'-TTCTTCCTCCTGCTGGTGGCG-3', Jh5 reverse 5'-CTCCCCGGCTTTCTTTCCTG-3'. The conditions for PCR amplification were 94^0 for 30sec, 60^0 for 30sec, 72^0 for 75sec, 25 cycles. The PCR products were then gel-purified with a QIAquick gel extraction kit (Qiagen, Manchester, UK) and cloned with the Zero Blunt TOPO PCR Cloning Kit (Thermo Scientific). Plasmid DNA extracted from individual bacterial colonies was sequenced in an automated sequencer. Mutations per base pair were calculated after aligning the V4-39-JH5 sequence from treated cells to the reference sequence (Supplementary Figure 2) using DNASTAR's SeqMan NGen software. At least 10,000 base pairs were assessed per experimental condition.

ChIP-Sequencing analysis of Lamin B1 binding

Chromatin immunoprecipitation (ChIP) was performed as described (16). BL2 cells were crosslinked with 1% paraformaldehyde for 5 minutes at room temperature. Paraformaldehyde was then quenched with glycine, and cells were harvested and sonicated using Bioruptor Plus (Diagenode) 5-8 cycles 30 second active/30 second inactive pulses to produce soluble ~ 300 bp chromatin fragments. Lamin B1 and control IgG ChIP-Seq was performed on two independent biological replicates with corresponding inputs per each

condition (control and SHM-induced), and then antibody-bound chromatin was immobilised with anti-rabbit IgG-conjugated Dynabeads (112.04D, Invitrogen, UK). DNA libraries were prepared using Illumina Nextera DNA Library Preparation Kit (FC-121-1030), and then massive parallel sequencing was performed using Illumina HiSeq2500 sequencer, yielding ~ 70 mln to 90 mln raw reads per sample.

Massively parallel sequencing and bioinformatical data analysis

Raw reads were mapped to the human genome (hg19) using the Bowtie 2 alignment software (21). Alignment BAM files were sorted by coordinates, and PCR duplicates were removed using Picard's MarkDuplicates program. To avoid any normalization bias, each pair of aligned input and ChIP BAM files were further processed to have the same read depth, using Picard's DownsampleSam program on the larger of the two files. Lamin B1 enriched regions were defined using the enriched domain detector algorithm (EDD) as described (22). The aligned peaks were then visualised using the Interactive Genome Browser (IGV, Broad Institute, Cambridge, Massachusetts) (23). Complete ChIP-Seq datasets are available at Gene Expression Omnibus (GEO) with accession number GSE89869.

LMNB1 RNAi experiments

For LMNB1 RNAi transfections, 50 nM siRNA was electroporated into 10^6 of logarithmically growing BL2 cells using Lonza Nucleofector 2b device (Basel, Switzerland), nucleofection solution T and C009 programme. After electroporation, cells were resuspended and immediately seeded into a pre-warmed fresh growth medium at $0.25x10^6$ cells/ml concentration. Total and incorporated Lamin B1 levels were assessed by WB or ImageStream cytometry 48 hours after electroporation. siRNAs used for this study: siGENOME siRNAs were received from Dharmacon (GE Healthcare, Roserberg, Sweden) and target sequences were the following: siRNA1 – GAAGGAAUCUGAUCUUAAU, siRNA2 – CAACUGACCUCAUCUGGAA, siRNA3 – GAAAGAGUCUAGAGCAUGU.

GCAUGAAACGCGCUUGGUA. ON-TARGETplus Non-targeting Control siRNA Pool (D-001810-10-05, Dharmacon) was used at 50 nM as an off-target siRNA control.

Microscopy and image analysis

For immunofluorescence microscopy, harvested cells were cytospun onto poly-l-lysine–coated microscope slides (suspension cells) or mouse spleens were cryosectioned using Leica CM3050 cryostat. Slides were fixed in –20°C methanol and then rinsed briefly in ice-cold acetone. Slides were washed in TBS/0.05% Tween and then incubated with appropriately diluted primary antibodies for 60-120 minutes at room temperature. The primary Abs were diluted in TBS/0.1% BSA. Subsequently, slides were washed x3 in TBS-Tween and stained using the anti-rabbit Alexa Fluor 488, anti-mouse Alexa Fluor 594 or anti-rat Alexa Fluor 594 (all Abcam). After three washes in TBS/0.05% Tween-20, DNA was counterstained with Propidium Iodide or DAPI before mounting in ProLong Gold Antifade Reagent (Invitrogen). Images were collected using a Nikon Ci-L Upright fluorescence microscope and NIS Elements software. In situ fluorescence intensity was measured within the linear fluorescence range, using MetaMorph software and integrated morphometry analysis module.

Primary antibodies used for immunofluorescence: rabbit anti-Lamin B1 (Abcam, ab16048), mouse anti-CD27 (BioLegend, 356401), rat anti-mouse IgD (Southern Biotech, 1120-01), rat anti-CD45R (B220) (Abcam, ab64100).

High throughput ImageStream cytometry

For Image Stream Cytometry, cells were fixed in -20^{o}C methanol, washed x3 in PBS and then non-specific binding was blocked using a 5mL of PBS/0.05% Tween/2% Foetal Calf

Serum (FCS). Cells were then stained rabbit anti-Lamin B1 antibody (Abcam, ab16048) in PBS/Tween/2%FCS for 60 minutes. The concentration of primary antibody was calibrated to keep the acquired fluorescence within the linear dynamic range. After three washes, cells were then stained with anti-rabbit Alexa Fluor 488, washed again, and then DNA was counterstained with DAPI. High throughput images were acquired using ImageStream X Mk II imaging cytometer, and Lamin B1 parameters were analysed using Excel software.

Flow cytometry of plasma membrane surface immunoglobulins.

To label cell surface immunoglobulins, cells were washed in PBS and resuspended in PBS/5% FCS containing fluorochrome-labelled anti-Ig antibodies. After 1 hour incubation, cells were washed in PBS, fixed in 2% paraformaldehyde for 20 minutes, washed again and assessed by FACScalibur analyser (BD Biosciences). Isotype and fluorochrome-matched non-targeting antibodies, added at equal concentrations, were used to set the background fluorescence. The following BioLegend (BioLegend UK, London) antibodies were used in this study: PE anti-human Ig light chain λ (316607), PE Mouse IgG2a, κ Isotype Ctrl (FC) (400213), PE anti-human Ig light chain κ Antibody (316507), PE Mouse IgG1, κ Isotype Ctrl (FC) Antibody (400113),FITC anti-human IgD Antibody (348205), FITC Mouse IgG2a, κ Isotype Ctrl (FC) Antibody (400209). FITC Fab2 anti-human IgG (F0185), RPE Fab2 anti-human IgM (R5111), and corresponding isotype controls (Control Reagent, Rabbit F(ab')2/FITC, X0929, and Control Reagent, Rabbit F(ab')2/RPE, X0930) were obtained from Dako (Agilent Technologies, Cheadle, UK).

Cell proliferation assay

Cell proliferation was assessed by FACS using Click-iT Plus EdU Flow Cytometry or by fluorescence microscopy using Click-iT EdU Alexa Fluor 488 Imaging Kits (Invitrogen/Thermo-Fisher, Paisley, UK). 10 μM EdU was added to growing cells for 2

(LMNB1 siRNA experiments) or 16 (assessment of steady-state proliferation) hours and then cells were processed essentially according to manufacturer's protocols.

Western blotting

Whole cell lysates were prepared in NuPage LDS sample buffer (Thermo-Fisher, Paisley, UK), containing 0.1 M DTT. Samples were then separated by using 4-12% or 10% pre-cast NuPAGE Novex gels (Thermo-Fisher, Paisley, UK), and proteins were transferred onto PVDF membrane using a wet transfer system (BioRad, Hemel Hempstead, UK). Membranes were blocked with 5% non-fat dried milk in TBS/0.05% Tween, incubated with the appropriately diluted primary antibodies, washed, incubated with horseradish peroxidase–conjugated anti-rabbit, anti-mouse IgG (GE Healthcare/Amersham, Little Chalfont, UK) or anti-rat (DAKO/Agilent, Stockport, UK), and visualized by ECL (GE Healthcare/Amersham, Little Chalfont, UK) and ChemiDoc imaging system (BioRad, Hemel Hempstead, UK). Primary antibodies used for WB: rabbit anti-Lamin B1 (Abcam, ab16048), rabbit anti-histone H3 (Abcam, ab1791), mouse anti-Bcl6 (Active Motif, 61194), Rat anti-AID (Active Motif, 39886).

Animal immunisation

C57BL/6 mice were immunised by IP injection with 10 ng LPS plus 0.5 mg ovalbumin (SIGMA) in 200ul PBS. 7 or 14 days later mice were sacrificed, spleens removed and processed for IHC/IF or the homogenised and the Germinal Centre B cells were isolated by MACS using a Mouse Germinal Center B Cell (PNA) MicroBead Kit (Miltenyi Biotec, Bisley, UK). Animals were maintained in local facilities and experiments approved by local ethical committees under Home Office license PPL30/2964.

Taqman qRT-PCR gene expression analysis

For cell line, genomic DNA and total RNA were purified using AllPrep DNA/RNA mini kit (Qiagen) as per manufacturer instructions. Total RNA from primary B-cells isolated from mouse spleens was purified using RNeasy mini kit. To remove DNA contaminations, all RNA samples were treated on-column with the QIAGEN RNase-Free DNase; purified RNA was quantified with Qubit® RNA BR (Broad-Range) Assay Kit (Thermofisher) and reverse transcribed using High-Capacity RNA-to-cDNA™ Kit (Applied Biosystems) according to manufacturer instructions. Triplicate amplification reactions containing 15-50 ng or input RNA each were carried out. TaqMan probes used in this study are listed in Supplementary table 1. mRNA encoding ribosomal protein S18 and β-actin were used as the standard internal controls. Reaction mixes (20 µl) contained TaqMan® Gene Expression Master Mix 1x, TagMan Gene Expression Assay 1x and template cDNA. qPCR reactions were performed and analysed on an Applied Biosystems ABI QuantStudio7 using ddCt comparison method. Graphing and statistical analyses were performed using GraphPad Prism 7. All three groups were compared to each other by one-way ANOVA with Tukey's post-test.

Patients and samples

Expression profiling was conducted on peripheral blood samples from 337 previously untreated CLL patients. Samples were collected at enrolment on the CLL8-trial, a prospective, international, multicenter trial comparing first-line treatment with FC or FCR in a 1:1 randomized fashion (www.clinicaltrials.gov NCT00281918) as previously described (24). Ficoll density gradient centrifugation for isolation of mononuclear cells followed by an immunomagnetic tumor cell enrichment via CD19 (Midi MACS, Miltenyi Biotec, Bergisch Gladbach, Germany) was performed on all samples. Data on genomic aberrations (del(11)(q22.3), +12, del(13)(q14), del(17)(p13), t(11;14)) the IGHV, TP53, SF3B1 and

NOTCH1 mutational status was assessed as previously described (24, 25). Written informed consent and local ethics committee approval was obtained in accordance with the Declaration of Helsinki for all patients.

Gene expression profiling on BL2 cell line was conducted for 2 independently cultured passages with 4 experimental approaches each, with 1) control with non-targeting siRNA 2) control with non-targeting siRNA and after induction of SHM 3) LMNB1 RNAi transfected 4) LMNB1 RNAi transfected and after induction of SHM. For siRNA treated samples, SMARTpool LMNB1 siRNA mixture of three siRNAs in equimolar concentration was used.

RNA isolation and quality assessment

Total RNA for mRNA profiling was extracted from whole cell lysates of treated BL2 cells and primary patient samples according to the Allprep DNA/RNA mini kit (Qiagen). Quality control was assessed using the Agilent 2100 Bioanalyzer with the RNA 6000 Nano LabChip (Agilent Technologies). The Chip was prepared according to the manufacturer's protocol and analyzed using the 2100 Expert software. To secure the best accuracy and reproducibility samples with an RNA Integrity Number (RIN) less than 7.0 were excluded from further analysis. RNA for gene expression profiling on BL2 cell line functional studies had a RIN of 10.

Gene expression profiling on Exon ST 1.0 Arrays

Patient samples and samples from functional studies on BL2 cells were analyzed for mRNA expression using the Affymetrix GeneChip® Human Exon 1.0 ST Array (Affymetrix, Santa Clara, CA, USA). The experiment was conducted according to the manufacturer’s protocol. In brief, 250 ng RNA per sample were amplified, transcribed to cDNA, fragmented and

subsequently labeled with Biotin. Array hybridization was performed at 45°C for 16-18h in the Affymetrix GeneChip® Hybridization Oven 640, arrays were subsequently washed in the Fluidics Station 450 and scanned on the GeneChip scanner 3000 7G. Complete GEP datasets are available at Gene Expression Omnibus (GEO) with accession number GSE98529.

Normalization and analysis of expression data

Statistical procedures were performed with the R software version 2.15.1 and BRB-ArrayTools Version: 4.2.1 Raw Affymetrix Human Exon array (HuEx-1_0-st-v2) data files have been preprocessed by the robust multichip average (RMA) algorithm using either the implementation in the R-package *oligo* (26) or *aroma.affymterix* (University of California, Berkeley 2008). Besides RMA normalization the default background correction and quantile normalization was applied. *Aroma.affymterix* was applied to generate gene expression values summarized on the exon/probe set level and on the transcript level using the 'core' probe set definition according to Affymetrix. Hierarchial clustering on selected genes was conducted using the "Genesis platform" (27) using pearson correlation and average linkage as agglomeration rule and distance metric, respectively. Gene Set Enrichment Analysis (GSEA) (28) was performed on "C7: immunologic signatures" gene sets compiled at the Molecular Signatures Database, Broad Institute.

Statistical methods

Standard statistical means were used to evaluate associations between clinical and molecular patient characteristics (χ^2/Fisher's exact; Mann-Whitney/Kruskal-Wallis). Time-to-event parameters included PFS and OS, and were estimated by the Kaplan-Meier method. Survival times were compared via two-sided non-stratified log-rank tests. Hazard ratios (HR) were calculated using Cox proportional-hazard regression analyses. All tests were two-

sided, and a P value <.05 was defined as statistically significant. No adjustments for multiple tests were performed. Statistical analyses were performed with SPSS v23 (SPSS, Chicago, IL).

Results

To evaluate Lamin B1 dynamics in secondary lymphoid tissues, we performed IHC staining for Lamin B1 in spleens of OVA-challenged mice on day 14 post-immunisation, when the amount of germinal centres (GC) per spleen was maximal (Figure 1A), accompanied by an average of six-fold increase in GL7+ splenocytes (Supplementary figure 1A and B). We observed a consistent reduction of nuclear Lamin B1 within Peanut-Agglutinin (PNA) visualised GC cells but not Mantle Zone (MZ) B cells (Figure 1B and C) or follicular T cells (not shown).

Complementary to spatial analysis of Lamin B1 in spleens of OVA-immunised animals, we then MACS separated PNA+ splenocytes and performed qRT-PCR analysis of LMNB1 gene expression in PNA+ vs PNA- fractions. Figure 1D demonstrate that mRNA levels of LMNB1 were invariably decreased in PNA+ fraction. In contrast, expression of both mKI67 and TNFR6 were elevated in PNA+ cells, consistent with their biological function in activated murine B cells. Next, we tested whether reduction of LMNB1 gene expression (Figure 1D) translates into a reduced nuclear incorporation of Lamin B1 protein in PNA+ splenocytes. Figure 1E and F, and Supplementary figure 1C clearly demonstrate that, as compared to PNA-depleted fraction, nuclear Lamin B1 fluorescence is significantly decreased in PNA+ cells.

To test whether the decrease in Lamin B1 was a general cross-species phenomenon related to GC formation, we next assessed a panel of tissue microarrays (TMAs) containing 42 human biopsies with previously diagnosed reactive lymphoid hyperplasia. Microscopic studies, accompanied by image analysis revealed a consistent decrease in nuclear Lamin

B1 within the intrafollicular areas (as assessed by Ki67 staining) of reactive lymph nodes, compared to extrafollicular IgD+ mantle zone areas (Supplementary figure 1D and E). These results demonstrate a general decrease in Lamin B1 during GC formation in humans and mice.

We next hypothesised that the observed decrease in GC Lamin B1 might be associated with a specific change in GC B cells. After antigen engagement, activation and several rounds of cell division, B cells undergo SHM; a process by which the antibody-encoding DNA sequences are mutated at a highly elevated frequency, generating a diverse series of clones in the GC. We therefore tested whether induction of SHM was associated with a decrease in nuclear Lamin B1. For this purpose, we used BL2 cells, a human B-cell line used previously as a model for assessing SHM (20). Parallel assessment of Lamin B1 nuclear incorporation by ImageStream and in situ cytometry revealed a robust reduction of Lamin B1 at the nuclear periphery in cells undergoing SHM (Figure 1, G and H).

Keeping in mind the previously reported role of Lamin B1 in the LAD-mediated epigenetic regulation of chromatin, we hypothesised that Lamin B1 might be a mutational “gatekeeper”, maintaining the IgH V gene clusters within the restrictive facultative heterochromatic regions. Upon antigen stimulation, these genome segments can be released from the suppressive environment of the nuclear lamina, followed by access for transcription and, potentially, mutations. In support of this hypothesis, analysis of previous chromatin immunoprecipitation (ChIP) studies performed in primary fibroblasts (15, 16) revealed that LADs precisely co-localise with all three (kappa, lambda, heavy) Ig variable gene clusters (Supplementary figure 2). This observation suggests that IgV gene clusters can be prime candidates for epigenetic regulation via LADs.

To address our hypothesis more directly, we next performed ChIP-sequencing analysis of Lamin B1 genome binding in the human BL2 cells undergoing SHM. Our analysis revealed that in control cells the topology of Lamin B1 binding (defined as LADs according to our previously used algorithms (29)) precisely coincide with the IgV clusters. Induction of SHM resulted in a rearrangement of Lamin B1 binding to the genome with a general drop of its binding to chromosomes 1 to 14 and increased binding to smaller chromosomes 15 to 22 (Supplementary figure 3A). On that background, Lamin B1 "canyons" – areas of decreased genome binding - invariably coincided with IgV gene clusters, even if surrounded by "mesas" – areas of increased Lamin B1 binding after SHM induction (Supplementary figure 3B).

Most importantly, results displayed in Figures 1I and J indicate that, after stimulation, mutations in a 565 bp reporter fragment of the V4-39-J_h5 gene increases ~4.5 fold (Figure 1I and Supplementary figure 4). Furthermore, 85% of nucleotide substitutions are consistent with AICDA-dependent cytidine deamination within the WRCY motif, a functional hallmark of SHM (Supplementary figure 4C). This increased mutational load (Figure 1I) was accompanied by a gross three-fold, yet precise reduction of Lamin B1 binding to this fragment after SHM induction (Figure 1J). These data suggest a direct involvement of Lamin B1 in epigenetic regulation of SHM in IgV domains.

We next suggested that the decreased nuclear Lamin B1 could be associated with altered cell cycle redistribution which is a function of the proliferative capacity of cells. According to this hypothesis, cells that proliferate fast would have lower levels of nuclear Lamin B1, which in turn would be consistent with a higher proliferation rate of GC B cells in vivo, or activated BL2 or primary B cells in vitro. To address this hypothesis directly, we compared Lamin B1 levels within different cell cycle phases by FACS and immunofluorescence. Furthermore, we tested the correlation between the proportion of EdU positive cells and their Lamin B1 level

409 in six different cell lines under various growth conditions (Supplementary figure 5). These
410 experiments revealed no association between steady state cell proliferation and nuclear
411 Lamin B1 (Supplementary figure 5). In fact, more rapidly proliferating cells had a tendency to
412 increase their Lamin B1 incorporation (Supplementary figure 5A) due to the marginally
413 higher amount of Lamin B1 in G2, as compared to G1 cells (Supplementary figure 5, B and
414 C). Likewise, in situ cytometry showed no difference in Lamin B1 incorporation between
415 EdU positive and EdU negative cells (Supplementary figure 6, D and E). These results
416 suggest that a decreased Lamin B1 in germinal centre B cells is likely to be associated with
417 a more specific role which is not a passive reflection of cellular proliferation *per se*.

418

419 To test the impact of Lamin B1 on cell dynamics and SHM directly, we then transfected BL2
420 cells with siRNA targeting mRNA transcripts from three different exons of the LMNB1 gene
421 (See Materials and Methods). In general, 50 – 80% reduction of Lamin B1 protein level
422 (Figure 2A) 48 hours after siRNA electroporation translated to an average of 32% reduction
423 in Lamin B1 nuclear incorporation (Figure 2, B and C). Interestingly, this level of reduced
424 Lamin B1 incorporation was very similar to that produced by SHM induction (compare
425 Figures 1G and 2C), potentially suggesting a functional epigenetic compartment of nuclear
426 Lamin B1 different from its structural function.

427

428 Having established a specific RNAi-mediated reduction of nuclear Lamin B1, we next tested
429 whether Lamin $B1^{low}$ cells would exhibit any phenotypic features characteristic of GC B cells.
430 Our findings displayed on Figures 2 D and E demonstrate that proliferation boost, as
431 detected by on average 27% more EdU positive cells, was a characteristic feature of siRNA-
432 treated Lamin $B1^{low}$ cells. This proliferation boost was accompanied by a general
433 upregulation of positive cell cycle regulatory genes which, in turn, occurred alongside an
434 upregulation of genes responsible for cell cycle checkpoint execution or cell cycle arrest, and

were specific for LMNB1 reduction; independent of SHM induction (Figure 2F and Supplementary figure 6). We believe the latter can be interpreted as a secondary cellular response to uncontrolled proliferation and DNA lesions.

AICDA is a master regulator of antibody diversification at DNA level via SHM and class-switch recombination (30). AID expression peaks in GCs where it is positively regulated by BCL6 via an indirect miR-155-mediated mechanism (31). We set out to examine that upregulation of AID might be a primary mechanism for SHM induction by antigen ligation or LMNB1 siRNA. Figure 2G shows that neither AICDA nor its GC regulator BCL6 is induced by antibodies or LMNB1 siRNA. We therefore suggest that Lamin B1-mediated chromatin accessibility could be the primary factor regulating SHM in BL2 cells.

It is suggested that individual B-cells in lymphoid tissues possess either kappa or lambda light chains. A mixture of kappa and lambda positive cells is characteristic of reactive or otherwise benign GCs. Our previous immunophenotypic analysis of BL2 cells revealed strong lambda chain expression on the cell surface, which is likely to be due to BL2-specific t(8,22) translocation involving IGL@ locus. On the contrary, the non-rearranged kappa-light chain, expressed from chromosome 2, was largely absent from the cell surface. Consistent with our model, we found that IGK@ was heavily incorporated within the Lamin B1 binding sites. We next hypothesised that siRNA-mediated reduction of Lamin B1 incorporation would release the IGK@ locus from its suppressive environment that would result in *de novo* expression of kappa-light chain on the cell surface. In agreement with this hypothesis, decreasing Lamin B1 binding to the IGK@ locus (Supplementary figure 3B) was accompanied by ~ 5 fold induction of kappa light chain expression on the cell surface (Figure 2H).

Finally, we tested whether siRNA-mediated reduction of Lamin B1 incorporation results in spontaneous SHM. By analogy with Figure 1I, clonal analysis of the IGHV4-39 locus revealed a ~ 4-fold induction of spontaneous SHM in cells treated with smartpooled LMNB1 siRNA (Figure 2I) with 72.4% of nucleotide substitutions falling within the AICDA-related mutational hotspots (Supplementary figure 4D). Notably, combining LMNB1 siRNA treatment and induction of SHM by ligating surface antigens did not alter the SHM rate induced by siRNA-treatment alone. This suggests a shared cellular mechanism of SHM induction between nuclear lamina and external stimuli, resulting in a binary induction of SHM.

To further our functional evidence on the involvement of Lamin B1 in SHM, we next tested whether IGHV4-39 mutations occurring after LMNB1 RNAi treatment are AICDA dependent. To do this, we did similar LMNB1 RNAi treatments in AICDA-/- cells described previously (20). Figure 2J demonstrates that AICDA-/- background almost completely negates both background and LMNB1 RNAi induced mutations. Interestingly, although we couldn't detect any AICDA signal by qRT-PCR and Western blotting (Figure 2K and L), significant amount of AICDA expression could be observed in wt BL2 cells, which is in agreement with previously published reports (20, 32). Furthermore, it's expression did not significantly change after LMNB1 RNAi (Figure 2K) that, in combination with Figure 2G, suggests that other chromatin factors are at least as important in SHM as AICDA expression *per se*. Out data suggest that lamina mediated conformational changes could be one of these factors.

We were unable to establish a stable LMNB1 negative cell line using CRISPR/CAS9 or shRNA approach. Neither are we aware of the existence of any such human cell models, outside of cellular senescence.

Formation of plasma or memory cells is the outcome for B cells following SHM and clonal selection (33). Given the acute functional impact of Lamin B1 in our in vitro system, we

tested whether the drop in Lamin B1 in GC B cells translates into their ultimate differentiated state. If the GC-associated drop in Lamin B1 is transient, this might then suggest a temporary chromatin access for a naïve B cell to rearrange its Ig domains and, hence, fine-tune the antibody repertoire. To address this question, we first compared the expression of Lamin B1 in human $CD27^+$ vs. $CD27^-$ B cells within the GCs of fresh frozen human lymph nodes. CD27 is a widely accepted marker of memory B cells that can be detected in human GCs (34) before GC-dependent memory cells relocate to the marginal zone (35, 36). Figure 3 A-C demonstrates that $CD27^+$ cells have a substantially higher expression of Lamin B1 compared to $CD27^-$ GC B cells. These data suggest that the drop in Lamin B1 is transient and is only temporally associated with SHM in normal B cells.

Although the cellular origin of chronic lymphocytic leukaemia (CLL) is still debated, several lines of evidence suggest that CLL cells are antigen-experienced (37), resembling memory B cells (38). Within this context, IGHV-mutated CLL cells, associated with favourable clinical prognosis and derived from the CD5+/CD27+ post–germinal centre B cell subset, could be similar to “classic memory B cells” generated by a typical GC-based reaction, represented in our system as a CD27+ GC B cells (Figure 3 A-C).

By analogy with the normal CD27+ memory B cells, we hypothesised that IGHV-mutated CLL (mCLL) would be associated with higher Lamin B1 expression levels as compared to unmutated CLL cases (uCLL). Furthermore, given an association of IGHV mutational status with clinical outcome, we anticipated that Lamin B1 would *per se* constitute a prognostic factor in CLL.

With that in mind, we analysed gene expression profiles of 337 previously untreated CLL patients, enrolled on the CLL8 trial evaluating FC versus FCR in a randomised fashion

(NCT00281918) (24, 39) . As implicated from our functional studies, higher *LMNB1* expression, as dichotomised at the median (LMNB1 low ≤ 6.51 vs LMNB1 high > 6.51), was inversely correlated with high-risk genomic aberrations (Supplementary table 2) and was associated with shorter median progression-free (PFS) survival (32.4 vs. 49.9 months, p = 0.010) and, notably, overall (OS) (83.6 months vs. not reached, p = 0.001) and (Figure 3, D and E).

Conversely, we were unable to detect a similar clinical impact for LMNB2 and LMNA genes (Supplementary figure 7), encoding two other components of the nuclear lamina, Lamin B2 and Lamin A/C respectively. The latter highlights a highly specific impact of Lamin B1 in the molecular pathology of CLL.

Moreover, univariate Cox regression analysis comparing low (≤ 6.51) and high (> 6.51) LMNB1 expression cohorts revealed an overall hazard ratio (HR) of 0.715 for PFS and 0.551 for OS (95% CI) (Figure 3F), suggesting a strong protective impact of LMNB1 expression in CLL. Interestingly, further stratification of patients according to their treatment regime revealed a very similar LMNB1-related HR regardless of the therapeutic modality applied (Figure 3F). The latter suggests that the molecular mechanisms responsible LMNB1-mediated protection of CLL patients are different from the mechanisms covered by chemotherapy.

Further, we were able to solidify functional model derived clinico-biologic implications in the context of CLL. First, we correlated LMNB1 expression from our datasets with the total amount of Lamin B1 protein, and, although not absolute, a positive correlation between gene expression and protein content could be observed (Supplementary figure 8A). Next, when performing gene set enrichment analysis for CLL cases dichotomized for lower and upper

quartiles of LMNB1 expression, we found “LMNB1 quartile low” cases to extensively match signatures of anti-IgM activated B cells (Supplementary figure 8B) while there was only a 1.12-fold expression change for AID observable for “LMNB1 quartile low” expressing CLLs (data not shown). This suggests that CLL cells with LMNB1 downregulation are transcriptionally locked in an activated state. Complementary to this, and resembling LMNB1 siRNA phenotype in BL2 cells, we found an inverse relationship between expression of LMNB1 and expression of positive cell cycle regulatory genes (Supplementary figure 8B). On that background, low LMNB1 expression was also strongly associated with high BCL2 and low CDKN1A expression levels (Supplementary figure 8B), further highlighting similarities between Lamin $B1^{low}$ and GC B cells.

We next assessed whether differential expression of LMNB1 in CLL can be attributed to differential CpG methylation within this gene. Given a strong association of LMNB1 expression with IGHV mutational status, we next compared the methylation values (normalized Infinium HumanMethylation450 BeadChip beta values) for LMNB1 promoter CpG sites between CLL patients with mutated and non-mutated IGHV. Two sample t-test with equal variances revealed no association between LMNB1 methylation and IGHV mutational status, suggesting that mechanisms other than CpG methylation are responsible for regulating LMNB1 expression in CLL (Supplementary figure 9).

We next hypothesised that a permissive chromatin state, associated with decreased nuclear Lamin B1 in GC B cells, might be linked to secondary “off target” mutation events. The latter can be followed by a formation of malignancies that originate in the GC such as Follicular Lymphoma (FL) or Diffuse Large B Cell Lymphoma (DLBCL). In support of this hypothesis, we found a consistently decreased amount of Lamin B1 in the majority of primary lymphoid tumours, as compared to intrafollicular areas of normal human reactive lymph nodes (Figure

4, A and B). Intriguingly, we found decreased Lamin B1 in other non-lymphoid malignancies including acute myeloid leukaemia (AML) demonstrating that LADs are also deregulated in other haematological malignancies (Figure 4A). Next, we assessed a chronological series of biopsies from 43 patients with FL, which subsequently underwent transformation. We found that FL transformation was strongly associated with a further decrease in Lamin B1 (Figure 4, C and D), suggesting a possible involvement of LADs in the progression of this malignancy.

Discussion

One of the principal questions in B cell biology yet to be answered is how SHM machinery accesses immunoglobulin loci. For SHM to take place, Ig variable loci should be subjected to AID-mediated deamination as well as DNA cleavage and repair. Each of these events is likely to be regulated by specific changes in chromatin, resulting in its open and accessible conformation. In resting B cells, most of the IgH locus exist in a closed chromatin state, enriched in repressive histone marks, such as H3K9Me3 and H3K27Me3 (40), as well as HP1-γ protein (41). Within that context, it is intriguing that both H3K9Me3 and HP1-γ are known to be associated with Lamin B1 (42), topologically defining lamina-associated chromatin domains (10, 16).

In this study, we show that perinuclear Lamin B1 is decreased in germinal centres of mouse and human lymphoid follicles. The reduction of nuclear Lamin B1 could also be observed after induction of SHM in vitro. This was accompanied by the reduced genome binding of Lamin B1, including the domains that encode variable immunoglobulin parts. Furthermore, the clonal analysis revealed that the rate of SHM was grossly increased when Lamin B1 genome incorporation was suppressed by RNA interference, providing for the first time a direct functional link between SHM and structural components of the nuclear envelope.

590 Downstream of GC, we found that Lamin B1 levels were restored in CD27+ memory B cells
591 indicating the temporary nature of Lamin B1 decrease in activated B cells. This suggests an
592 “epigenetic window of opportunity” for a GC B cell to start and complete SHM when the
593 chromatin state is permissive.

594

595 Interestingly, Lamin B1 dynamics in GC/post-GC B cells translates into CLL, which is a post-
596 GC malignancy. In particular, IGHV-mutated CLL cells, associated with a favourable clinical
597 prognosis and derived from the CD5+/CD27+ post–germinal centre B cell subset (43)
598 displayed significantly higher LMNB1 gene expression as compared to uCLL samples.
599 Furthermore, low LMNB1 expression was strongly associated with multiple cytogenetic
600 abnormalities and was a strong negative prognostic factor for both progression-free (PFS)
601 and overall survival (OS). The strong direct relationship between the LMNB1 expression
602 quartiles and survival (both OS and PFS) was independent of the treatment applied,
603 suggesting a novel mechanism of molecular pathogenesis of CLL, which is beyond control
604 by the currently available CLL treatment modalities. Targeting LaminB1-associated
605 mechanisms in CLL may provide another step towards the post-chemotherapy era and
606 complement existing therapies, potentially gaining even larger therapeutic margins for this
607 disease. Since low LMNB1 expression was strongly associated with clinically adverse
608 cytogenetic abnormalities, it is also tempting to speculate that, due to its proximal role in the
609 nuclear structure and function, Lamin B1 may serve as a safeguard against chromosomal
610 aberrations during the clonal evolution of CLL.

611

612 Deletions of 13q and 11q represent the most frequent and co-occurring aberrations in CLL
613 (25) and loss of the *DLEU2/miR-15a/16-1* cluster on 13q14 in mice is sufficient to initiate B-
614 cell lymphoproliferative disorders with CLL-like phenotypes (44). Moreover, deletion 13q and
615 trisomy 12, followed by deletion 11q, have been identified as early drivers in the evolutionary

process of CLL (45). Therefore, we hypothesise that the observed significant drops in Lamin B1 binding upon induction of SHM especially on chromosomes 13 and 12, or with slightly lesser extend on chromosome 11, may constitute the central selective vulnerability for deleterious hits initiating the development of CLL.

In line with this suggestion, defects of Lamin B1 expression and processing have previously been linked to aberrant interphase chromosome positioning (46) and chromatin instability (47) – a potential path to chromosomal aberrations. However, a direct functional link between LMNB1 expression and chromosomal abnormalities is yet to be established.

Here we also show that nuclear Lamin B1 is decreased in the majority of GC-derived lymphomas. Furthermore, sequential biopsies from individuals with transformed FL showed a noticeable decrease of perinuclear Lamin B1 content during FL transformation. The latter, unlike in CD27+ memory B or mCLL cells, suggests a GC-based clonal selection of Lamin $B1^{low}$ B cells with their subsequent propagation into lymphoma cells, presumably due to increased mutational load associated with more permissive chromatin state. From a translational perspective, reduced levels of Lamin B1 in follicular lymphoma could be developed into a robust molecular biomarker predicting transformation of indolent lymphoma. At the moment, despite major advances in technology, no biomarker other than histologic grade has proven to be sufficiently robust to be widely accepted clinically (48).

Overall, here we propose that Lamin B1 is an upstream epigenetic regulator of SHM in germinal centre B cells. Functionally, activation of GC B cells is associated with a drop in Lamin B1 and release of unrearranged IgV chromatin domains from the restrictive influence of LADs, in turn, enabling normal SHM to occur. Finally, we suggest that this permissive chromatin state also increases the likelihood of “off target” hits that ultimately contribute to

642 the formation and progression of GC lymphomas and, at the post-GC level, Chronic
643 Lymphocytic Leukaemia. Figure 4E represents a principal schema, outlining the Lamin B1
644 dynamics in normal and malignant B cells.

645

646 Having suggested a functional involvement of Lamin B1 in SHM regulation and tumour
647 progression, there is a number of questions that are still outstanding and warrant further
648 investigation. Firstly, it will be important to understand how Lamin B1 is regulated within the
649 GCs. Our data suggest that differential mRNA expression could be one of these factors.
650 However, given a rather rapid reduction of Lamin B1 incorporation during SHM induction in
651 BL2 cells (in our system, as early as 90 min), one would suggest that post-translational
652 regulation, could be equally involved in the reduction of nuclear Lamin B1. Within that
653 context, it is possible that Lamin B1 phosphorylation by cdk1 and protein kinase C (49) is
654 one of the mechanisms for the rapid disassembly of nuclear Lamin B1 in GC B cells. Next,
655 since we were unable to identify DNA methylation as a source for the differential LMNB1
656 expression in CLL, establishing this mechanism would provide a novel insight into the
657 pathophysiology of this disease, with clear translational potential.

658

659 Finally, taking into account clear involvement of Lamin B1 in the pathophysiology of GC and
660 post-GC B cell malignancies, manipulating nuclear Lamin B1 levels could provide a novel
661 therapeutic approach to these tumours, beyond the treatment modalities based on
662 chemotherapy or monoclonal antibodies. Within this context, we believe that Lamin B1
663 phosphorylation and farnesylation would be the primary therapeutic targets to control the
664 dynamics of nuclear lamina in leukaemia and lymphoma.

665

666 **Author contributions**

AB and TK conceived and designed the study. TK, AI, JBlo, KC, EUV, AC and JE performed experiments. JBlo and SE analysed microarray data. AI, JG, MC, SS, MH supervised the study. JW and AI analysed ChIP-Seq data. JBa and SR performed statistical analysis. JS and TKW analysed CLL methylation data. AB wrote the manuscript.

Acknowledgements: The authors would like to thank Selene Sodini, Glen Nishku and Guisepina Manfredi for their technical assistance. We further thank all patients and their physicians for CLL8 trial participation and donation of samples. This study was supported by Kay Kendall Leukemia Fund (KKL1101) (AB), Cancer Research UK Centre Grant (C16420/A18066) (AB, JG). J.B. and S.S. are supported by funding from DFG (SFB1074 B2), EC TransCan (FIRE CLL) and BMBF (PRECISE). J.E. was supported by the German Research Foundation (ED 256/1-1). JCS was funded by Bloodwise (11052, 12036), the Kay Kendall Leukaemia Fund (873), Cancer Research UK (C34999/A18087, ECMC C24563/A15581), Wessex Medical Research and the Bournemouth Leukaemia Fund. We further thank all patients and their physicians for CLL8 trial participation and donation of samples. The authors report no conflict of interest.

References

1. Li G, Zan H, Xu Z, Casali P. Epigenetics of the antibody response. Trends in Immunol. 2013;34(9):460-70.
2. Woo CJ, Martin A, Scharff MD. Induction of somatic hypermutation is associated with modifications in immunoglobulin variable region chromatin. Immunity. 2003;19(4):479-89.
3. Odegard VH, Kim ST, Anderson SM, Shlomchik MJ, Schatz DG. Histone modifications associated with somatic hypermutation. Immunity. 2005;23(1):101-10.
4. Begum NA, Stanlie A, Nakata M, Akiyama H, Honjo T. The histone chaperone Spt6 is required for activation-induced cytidine deaminase target determination through H3K4me3 regulation. J Biol Chem. 2012;287(39):32415-29.
5. Kosak ST, Skok JA, Medina KL, Riblet R, Le Beau MM, Fisher AG, et al. Subnuclear compartmentalization of immunoglobulin loci during lymphocyte development. Science. 2002;296(5565):158-62.
6. Park SK, Xiang Y, Feng X, Garrard WT. Pronounced cohabitation of active immunoglobulin genes from three different chromosomes in transcription factories during maximal antibody synthesis. Genes Dev. 2014;28(11):1159-64.

7. Skok JA, Brown KE, Azuara V, Caparros ML, Baxter J, Takacs K, et al. Nonequivalent nuclear location of immunoglobulin alleles in B lymphocytes. Nature Immunol. 2001;2(9):848-54.
8. Gruenbaum Y, Margalit A, Goldman RD, Shumaker DK, Wilson KL. The nuclear lamina comes of age. Nat Rev Mol Cell Biol. 2005;6(1):21-31.
9. Mao YS, Zhang B, Spector DL. Biogenesis and function of nuclear bodies. Trends in Genetics. 2011;27(8):295-306.
10. Guelen L, Pagie L, Brasset E, Meuleman W, Faza MB, Talhout W, et al. Domain organization of human chromosomes revealed by mapping of nuclear lamina interactions. Nature. 2008;453(7197):948-51.
11. Reddy KL, Zullo JM, Bertolino E, Singh H. Transcriptional repression mediated by repositioning of genes to the nuclear lamina. Nature. 2008;452(7184):243-7.
12. Zullo JM, Demarco IA, Pique-Regi R, Gaffney DJ, Epstein CB, Spooner CJ, et al. DNA sequence-dependent compartmentalization and silencing of chromatin at the nuclear lamina. Cell. 2012;149(7):1474-87.
13. Peric-Hupkes D, Meuleman W, Pagie L, Bruggeman SW, Solovei I, Brugman W, et al. Molecular maps of the reorganization of genome-nuclear lamina interactions during differentiation. Mol Cell. 2010;38(4):603-13.
14. Meuleman W, Peric-Hupkes D, Kind J, Beaudry JB, Pagie L, Kellis M, et al. Constitutive nuclear lamina-genome interactions are highly conserved and associated with A/T-rich sequence. Genome Res. 2013;23(2):270-80.
15. Shah PP, Donahue G, Otte GL, Capell BC, Nelson DM, Cao K, et al. Lamin B1 depletion in senescent cells triggers large-scale changes in gene expression and the chromatin landscape. Genes Dev. 2013;27(16):1787-99.
16. Sadaie M, Salama R, Carroll T, Tomimatsu K, Chandra T, Young AR, et al. Redistribution of the Lamin B1 genomic binding profile affects rearrangement of heterochromatic domains and SAHF formation during senescence. Genes Dev. 2013;27(16):1800-8.
17. Chen H, Zheng X, Zheng Y. Age-associated loss of lamin-B leads to systemic inflammation and gut hyperplasia. Cell. 2014;159(4):829-43.
18. Kind J, Pagie L, Ortabozkoyun H, Boyle S, de Vries SS, Janssen H, et al. Single-cell dynamics of genome-nuclear lamina interactions. Cell. 2013;153(1):178-92.
19. Taddei A, Van Houwe G, Nagai S, Erb I, van Nimwegen E, Gasser SM. The functional importance of telomere clustering: global changes in gene expression result from SIR factor dispersion. Genome Res. 2009;19(4):611-25.
20. Faili A, Aoufouchi S, Gueranger Q, Zober C, Leon A, Bertocci B, et al. AID-dependent somatic hypermutation occurs as a DNA single-strand event in the BL2 cell line. Nat Immunol. 2002;3(9):815-21.
21. Langmead B, Salzberg SL. Fast gapped-read alignment with Bowtie 2. Nat Methods. 2012;9(4):357-9.
22. Sievers S, Sternkopf Lillebaek EM, Jacobsen K, Lund A, Mollerup MS, Nielsen PK, et al. A multicopy sRNA of Listeria monocytogenes regulates expression of the virulence adhesin LapB. Nucleic Acids Res. 2014;42(14):9383-98.
23. Robinson JT, Thorvaldsdottir H, Winckler W, Guttman M, Lander ES, Getz G, et al. Integrative genomics viewer. Nat Biotechnol. 2011;29(1):24-6.
24. Hallek M, Fischer K, Fingerle-Rowson G, Fink AM, Busch R, Mayer J, et al. Addition of rituximab to fludarabine and cyclophosphamide in patients with chronic lymphocytic leukaemia: a randomised, open-label, phase 3 trial. Lancet. 2010;376(9747):1164-74.
25. Stilgenbauer S, Schnaiter A, Paschka P, Zenz T, Rossi M, Dohner K, et al. Gene mutations and treatment outcome in chronic lymphocytic leukemia: results from the CLL8 trial. Blood. 2014;123(21):3247-54.
26. Carvalho BS, Irizarry RA. A framework for oligonucleotide microarray preprocessing. Bioinformatics. 2010;26(19):2363-7.

27. Sturn A, Quackenbush J, Trajanoski Z. Genesis: cluster analysis of microarray data. Bioinformatics. 2002;18(1):207-8.
28. Subramanian A, Tamayo P, Mootha VK, Mukherjee S, Ebert BL, Gillette MA, et al. Gene set enrichment analysis: a knowledge-based approach for interpreting genome-wide expression profiles. Proc Natl Acad Sci U S A. 2005;102(43):15545-50.
29. Dou Z, Xu C, Donahue G, Shimi T, Pan JA, Zhu J, et al. Autophagy mediates degradation of nuclear lamina. Nature. 2015;527(7576):105-9.
30. Chaudhuri J, Tian M, Khuong C, Chua K, Pinaud E, Alt FW. Transcription-targeted DNA deamination by the AID antibody diversification enzyme. Nature. 2003;422(6933):726-30.
31. Basso K, Schneider C, Shen Q, Holmes AB, Setty M, Leslie C, et al. BCL6 positively regulates AID and germinal center gene expression via repression of miR-155. J Exp Med. 2012;209(13):2455-65.
32. Faili A, Aoufouchi S, Flatter E, Gueranger Q, Reynaud CA, Weill JC. Induction of somatic hypermutation in immunoglobulin genes is dependent on DNA polymerase iota. Nature. 2002;419(6910):944-7.
33. Shlomchik MJ, Weisel F. Germinal center selection and the development of memory B and plasma cells. Immunol Rev. 2012;247(1):52-63.
34. Good-Jacobson KL, Shlomchik MJ. Plasticity and heterogeneity in the generation of memory B cells and long-lived plasma cells: the influence of germinal center interactions and dynamics. J Immunol. 2010;185(6):3117-25.
35. Dunn-Walters DK, Isaacson PG, Spencer J. Analysis of mutations in immunoglobulin heavy chain variable region genes of microdissected marginal zone (MGZ) B cells suggests that the MGZ of human spleen is a reservoir of memory B cells. J Exp Med. 1995;182(2):559-66.
36. Tarlinton D, Good-Jacobson K. Diversity among memory B cells: origin, consequences, and utility. Science. 2013;341(6151):1205-11.
37. Damle RN, Ghiotto F, Valetto A, Albesiano E, Fais F, Yan XJ, et al. B-cell chronic lymphocytic leukemia cells express a surface membrane phenotype of activated, antigen-experienced B lymphocytes. Blood. 2002;99(11):4087-93.
38. Klein U, Tu Y, Stolovitzky GA, Mattioli M, Cattoretti G, Husson H, et al. Gene expression profiling of B cell chronic lymphocytic leukemia reveals a homogeneous phenotype related to memory B cells. J Exp Med. 2001;194(11):1625-38.
39. Fischer K, Bahlo J, Fink AM, Goede V, Herling CD, Cramer P, et al. Long-term remissions after FCR chemoimmunotherapy in previously untreated patients with CLL: updated results of the CLL8 trial. Blood. 2016;127(2):208-15.
40. Chowdhury M, Forouhi O, Dayal S, McCloskey N, Gould HJ, Felsenfeld G, et al. Analysis of intergenic transcription and histone modification across the human immunoglobulin heavy-chain locus. Proc Natl Acad Sci U S A. 2008;105(41):15872-7.
41. Jeevan-Raj BP, Robert I, Heyer V, Page A, Wang JH, Cammas F, et al. Epigenetic tethering of AID to the donor switch region during immunoglobulin class switch recombination. J Exp Med. 2011;208(8):1649-60.
42. Ye Q, Worman HJ. Interaction between an integral protein of the nuclear envelope inner membrane and human chromodomain proteins homologous to Drosophila HP1. J Biol Chem. 1996;271(25):14653-6.
43. Seifert M, Sellmann L, Bloehdorn J, Wein F, Stilgenbauer S, Durig J, et al. Cellular origin and pathophysiology of chronic lymphocytic leukemia. J Exp Med. 2012;209(12):2183-98.
44. Klein U, Lia M, Crespo M, Siegel R, Shen Q, Mo T, et al. The DLEU2/miR-15a/16-1 cluster controls B cell proliferation and its deletion leads to chronic lymphocytic leukemia. Cancer cell. 2010;17(1):28-40.
45. Landau DA, Tausch E, Taylor-Weiner AN, Stewart C, Reiter JG, Bahlo J, et al. Mutations driving CLL and their evolution in progression and relapse. Nature. 2015;526(7574):525-30.

46. Malhas A, Lee CF, Sanders R, Saunders NJ, Vaux DJ. Defects in lamin B1 expression or processing affect interphase chromosome position and gene expression. J Cell Biol. 2007;176(5):593-603.
47. Butin-Israeli V, Adam SA, Jain N, Otte GL, Neems D, Wiesmuller L, et al. Role of lamin b1 in chromatin instability. Mol Cell Biol. 2015;35(5):884-98.
48. Casulo C, Burack WR, Friedberg JW. Transformed follicular non-Hodgkin lymphoma. Blood. 2015;125(1):40-7.
49. Mall M, Walter T, Gorjanacz M, Davidson IF, Nga Ly-Hartig TB, Ellenberg J, et al. Mitotic lamin disassembly is triggered by lipid-mediated signaling. J Cell Biol. 2012;198(6):981-90.

Figure Legends

Figure 1. Nuclear Lamin B1 is reduced in follicular germinal centre B cells and is associated with somatic hypermutation. (A) C57BL/6 mice were immunised with LPS plus ovalbumin (OVA), and 7 or 14 days later spleens were removed and processed for immunohistochemistry. Figure represents the average number of GCs per spleen (n=3) ± s.e.m. (B) and (C) Spleen GCs were stained with anti-Lamin B1 antibodies (AlexaFluor 488, green channel), Peanut Agglutinin (PNA) (Pacific Blue, blue channel), and anti-B220 or anti-IgD antibodies (AlexaFluor 594, red channel). Fluorescence intensity of the Lamin B1 channel (C, bottom image) was measured using MetaMorph image analysis software within (PNA+ areas) or outside (B220+ or IgD+ PNA- areas) the GCs. At least 10 GCs from three spleens were analysed, and their Lamin B1 fluorescence was compared to a similar number of randomly selected extra-GC areas of the same size. (D – F) C57BL/6 mice were immunised with LPS plus ovalbumin (OVA), and after 14 days, spleens were removed, and PNA+ cells were isolated using PNA positive separation MicroBead Kit. (D) Taqman qRT-PCR analysis showing relative LMNB1, TNFR6 and Mki67 mRNA level changes in PNA+ vs PNA- splenocytes. (E) After microbead separation, nuclear Lamin B1 incorporation was measured by in situ cytometry in PNA+ vs PNA- cells (n=3). (F) Representative Lamin B1 immunofluorescence (AlexaFluor 488, green) in PNA+ and PNA- cells in OVA immunised animals. Nuclei were counterstained with DAPI (Blue). (G) SHM was induced in BL2 cells according to the protocol (see Materials and Methods) and nuclear Lamin B1 was assessed 48 hours post induction by IF and ImageStream image cytometry. Total nuclear Lamin B1

832 levels were reduced by an average of 20%. (H) Line scan analysis by MetaMorph reveals an
833 average 53% reduction in nuclear envelope bound Lamin B1 in SHM induced cells, as
834 compared to control cell population. (G) and (H) are the representative images of five
835 independent experiments. (I) DNA from control or activated BL2 cells was isolated, cloned,
836 and then analysed for mutations within the IGHV4-39 gene as described in Materials and
837 Methods. The reference IGHV4-39 sequence and nucleotide substitution pattern after SHM
838 induction and LMNB1 RNAi are displayed in Supplementary figure 5. At least 10,000 base
839 pairs (bp) were analysed per condition, and the mutational load was expressed as mutations
840 per bp. n = 4, ± s.e.m. $p<0.01$. (J) ChIP-Seq analysis of the dynamics of Lamin B1 binding
841 to the IGHV4-39 gene following SHM induction. As compared to control cells, Lamin B1
842 binding to this gene was significantly reduced 48 hours after cell activation. BLAT alignment
843 represents the IGHV4-39 sequence where SHM was assessed by Sanger sequencing and
844 clonal analysis.

845

846 **Figure 2. RNAi-mediated reduction of nuclear Lamin B1 results in acute proliferation**
847 **boost, de-novo surface antigen expression and AICDA-dependent somatic mutations.**
848 (A) Three different LMNB1 mRNA targeting siRNAs were nucleofected into BL2 cells and
849 then total Lamin B1 protein level was assessed by Western blotting 48 hours post
850 electroporation. (B) and (C) High throughput Lamin B1 nuclear incorporation was assessed
851 by ImageStream cytometry 48 hours after siRNA treatment. At least 8,000 cells were
852 analysed per sample. (B) Representative cells showing Lamin B1 fluorescence within the
853 median of sample intensity distributions. (C) Histograms showing absolute value distributions
854 for non-targeting siRNA control (NTC) or LMNB1 siRNA treated cells. (D) and (E) EdU was
855 added to WT, NTC or siRNA-treated cells 72 hours post siRNA treatment for 2 hours and
856 then the proportion of EdU+ cells was assessed by FACS. (D) Representative EdU FACS
857 profile showing 33% proliferation boost in siRNA2, as compared to NTC treated cells. (E)
858 The average percentage of EdU+ cells from three independent experiments ± s.e.m. $p<0.02$.

(F) Expression profiles of cell cycle regulatory genes in SHM-induced and/or LMNB1 siRNA treated BL2 cells. (NTC: control with non-targeting siRNA; NTC SHM: control with non-targeting siRNA and after induction of SHM; LMNB1: LMNB1 RNAi transfected; LMNB1 SHM: LMNB1 RNAi transfected and after induction of SHM. Experiments were conducted in two independent BL2 cell passages indicated with "-1" and "-2" behind the experiment label. For siRNA treated samples, a SMARTpool LMNB1 siRNA mixture of three siRNAs (A-F), in equimolar concentration was used. (G) Western blot analysis of AID and BCL6 proteins in antibody- or LMNB1 siRNA-treated samples at 72-hour time point. Histone H3 was used as a loading control. (H) FACS analysis of Ig surface antigen expression. Surface IgG, IgM, IgD, as well as kappa and lambda-light chain expression was assessed 72 hours after cells were treated with NTC or SMARTpool LMNB1 siRNA. For FACS, a fluorophore and isotype-matched non-targeting antibody was used to set background fluorescence. A representative of three independent experiments. (I – K) Mutations targeted to V4-39-Jh5 fragment are AICDA dependent. (I) Western blot and (J) qRT-PCR analysis of AICDA expression in BL2 wt and BL2 AID-/- cells treated with non-target control (NTC) or LMNB1 siRNA. (K) Parental and AID deficient BL2 clone were treated with LMNB1 RNAi, and mutations induced in V4-39 gene were analysed by Sanger sequencing. * $p<0.05$, ** $p<0.01$. (L) Cells were treated with SMARTpool LMNB1 siRNA and then SHM was assessed 72h post transfection. For combined antibody/siRNA-treated samples, SHM was induced 48 hours after LMNB1 siRNA transfection, and then DNA was isolated 72 hours after initial treatment. Data represents the average of three experiments ± s.e.m. $p<0.01$.

Figure 3. Nuclear Lamin B1 levels are restored in memory B cells and low LMNB1 expression level is an adverse prognostic factor in CLL. (A) Fresh frozen normal human lymph nodes were fixed in -20^{o}C methanol and then stained with PNA (Blue), Lamin B1 (green) and anti-CD27 antibodies (Red). (B) A zoomed in the area of (A, square) representing differential Lamin B1 expression in CD27+ vs. CD27- cell. (C) High throughput

886 comparison of Lamin B1 levels in CD27+ and CD27- GC cells. Lymph nodes from three
887 patients were assessed and in total 50 randomly selected CD27+, and 50 randomly selected
888 CD27- GC cells were analysed using MetaMorph software. (D) and (E) showing Kaplan-
889 Meier estimates of Progression-free (PFS) (D) and overall (OS) (E) of CLL patients enrolled
890 on the CLL8-trial as a factor of LMNB1 expression, dichotomised by the median (>6.51,
891 N=168 and ≤6.51, N=169. (F) Univariate Cox regression analysis comparing low (≤6.51,
892 N=169) and high (>6.51, N=168) LMNB1 expressing CLL patients as a factor of the
893 treatment regime (FC or FCR) applied. * $p<0.05$, ** $p<0.01$, *** $p<0.001$.

894

895 **Figure 4. Nuclear Lamin B1 decreased in B cell lymphomas.** (A) Immunohistochemical
896 tissue microarray analysis of nuclear Lamin B1 in tissue biopsies of B cell malignancies
897 showing decreasing LMNB1 staining with increasing aggressiveness. (B) Representative
898 IHC images from the lymphoid tumour panel displayed in (A). The horizontal line represents
899 Lamin B1 immunoreactivity within the intrafollicular areas of benign reactive lymph nodes. At
900 least three samples were analysed per tumour type, and bars represent average H-score
901 values ± s.e.m. (C) Lamin B1 immunoreactivity in sequential biopsies from a FL patient
902 (upper image) that later underwent FL transformation (lower image). (D) Lamin B1 H-score
903 values of 43 FL biopsies and their transformed counterparts. Each line connects two
904 sequential biopsies from the same patient. (E) Lamin B1 dynamics within the context of B
905 cell natural development in secondary lymphoid organs. Upon antigen stimulation in
906 secondary lymphoid organs, mature naïve B cells undergo activation accompanied by a
907 series of complex processes including SHM and clonal expansion. Our data suggest that
908 specific reduction of nuclear Lamin B1 in GC B cells is instrumental for these processes.
909 Furthermore, our observations suggest that this low level of Lamin B1 is locked in B cell
910 malignancies arising from a corresponding B cell development stage.

911

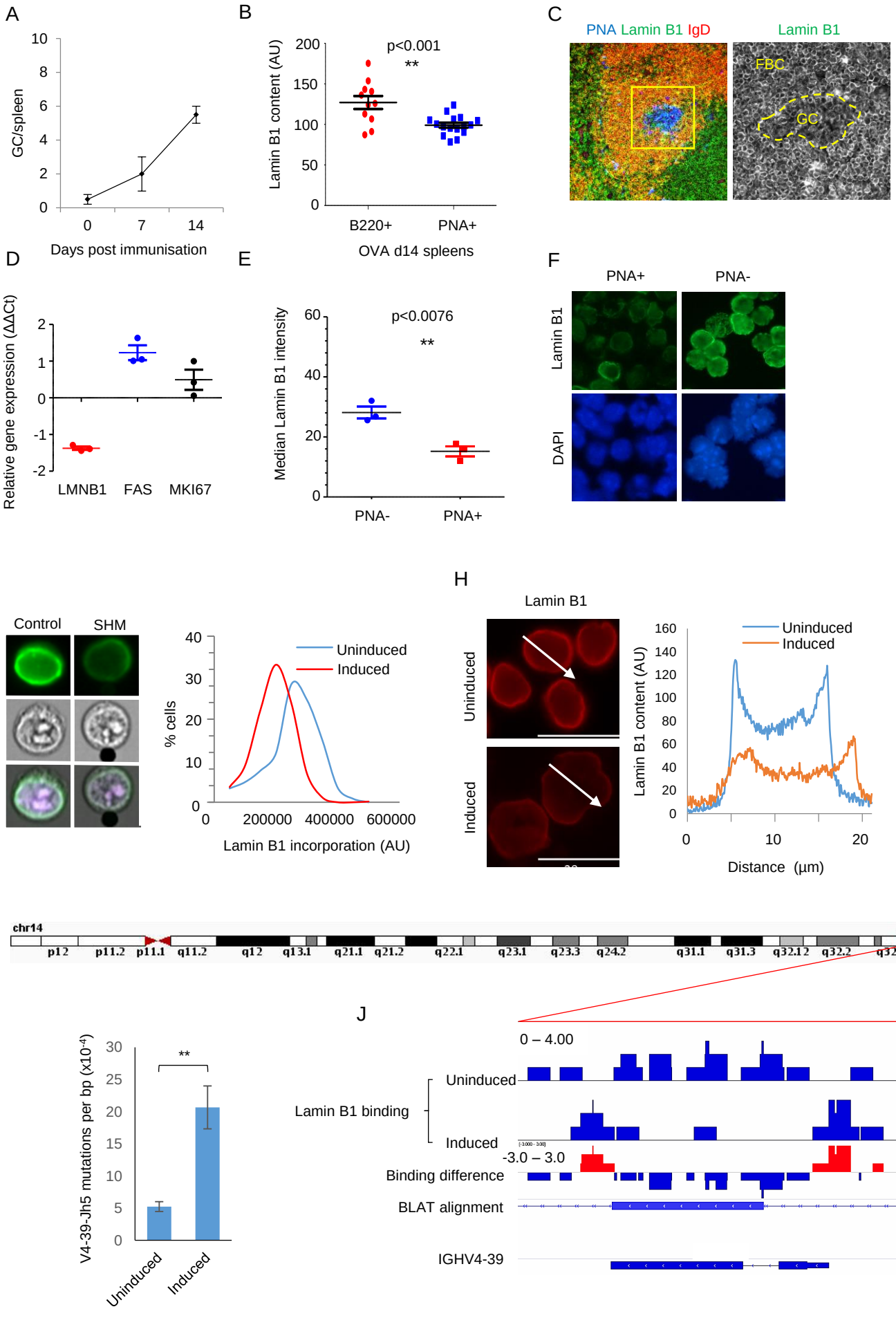
A
GC/spleen
Days post immunisation
B
Lamin B1 content (AU)
p<0.001
**
B220+
PNA+
OVA d14 spleens
C
PNA Lamin B1 IgD
Lamin B1
FBC
GC
D
Relative gene expression (ΔΔCt)
LMNB1
FAS
MKI67
E
Median Lamin B1 intensity
p<0.0076
**
PNA-
PNA+
F
PNA+
PNA-
Lamin B1
DAPI
G
Control
SHM
% cells
Uninduced
Induced
Lamin B1 incorporation (AU)
H
Lamin B1
Uninduced
Induced
Lamin B1 content (AU)
Distance (μm)
chr14
I
V4-39-Jh5 mutations per bp (x10⁻⁴)
**
Uninduced
Induced
J
0 – 4.00
Lamin B1 binding
Uninduced
Induced
-3.0 – 3.0
Binding difference
BLAT alignment
IGHV4-39

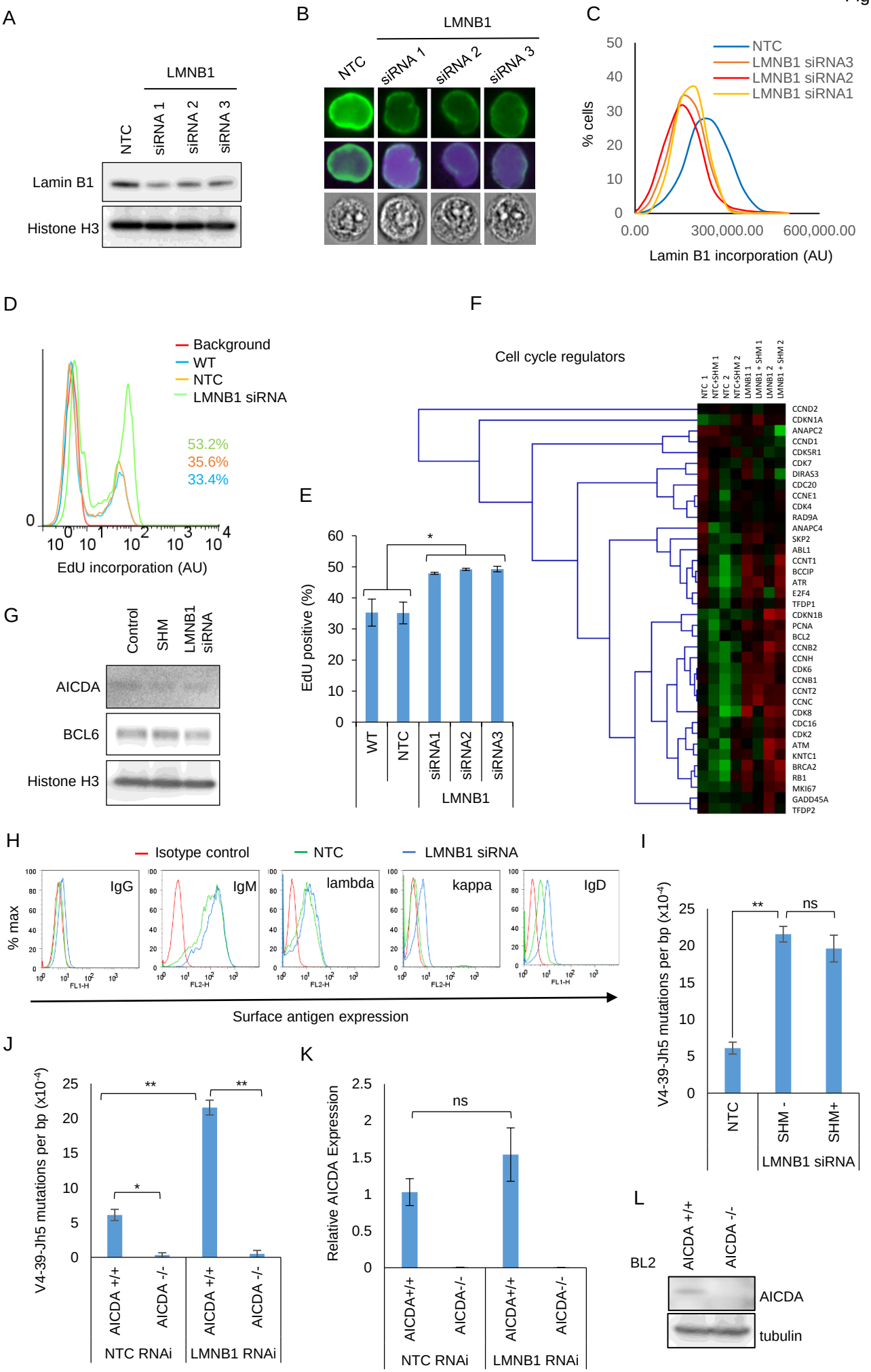
A
LMNB1
NTC
siRNA 1
siRNA 2
siRNA 3
Lamin B1
Histone H3
B
LMNB1
NTC
siRNA 1
siRNA 2
siRNA 3
C
NTC
LMNB1 siRNA3
LMNB1 siRNA2
LMNB1 siRNA1
% cells
Lamin B1 incorporation (AU)
D
Background
WT
NTC
LMNB1 siRNA
53.2%
35.6%
33.4%
EdU incorporation (AU)
E
EdU positive (%)
WT
NTC
siRNA1
siRNA2
siRNA3
LMNB1
F
Cell cycle regulators
G
Control
SHM
LMNB1 siRNA
AICDA
BCL6
Histone H3
H
Isotype control
NTC
LMNB1 siRNA
IgG
IgM
lambda
kappa
IgD
% max
Surface antigen expression
I
V4-39-Jh5 mutations per bp (x10-4)
ns
NTC
SHM -
SHM+
LMNB1 siRNA
J
V4-39-Jh5 mutations per bp (x10-4)
AICDA +/+
AICDA -/-
NTC RNAi
LMNB1 RNAi
K
Relative AICDA Expression
ns
L
BL2
AICDA +/+
AICDA -/-
AICDA
tubulin

A

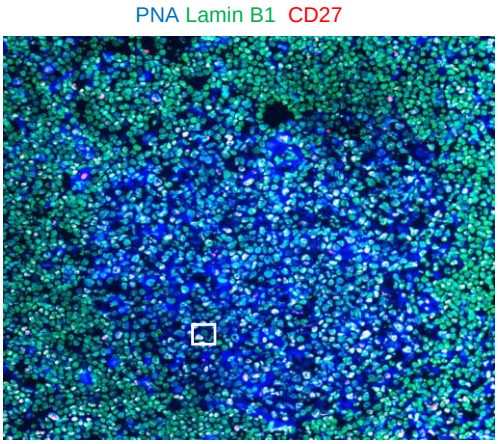
PNA Lamin B1 CD27

B

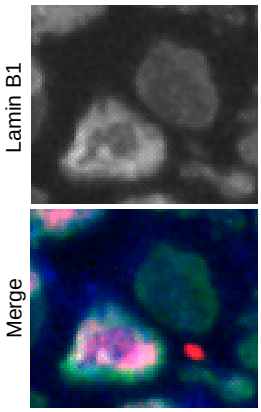
Lamin B1
Merge

C

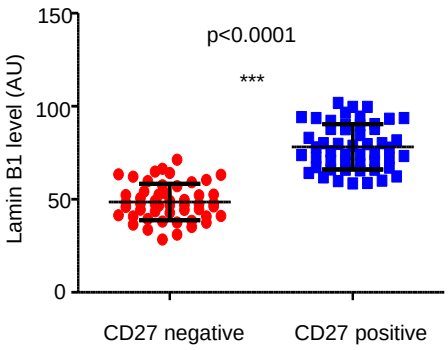
p<0.0001
***
Lamin B1 level (AU)
150
100
50
0
CD27 negative
CD27 positive

D

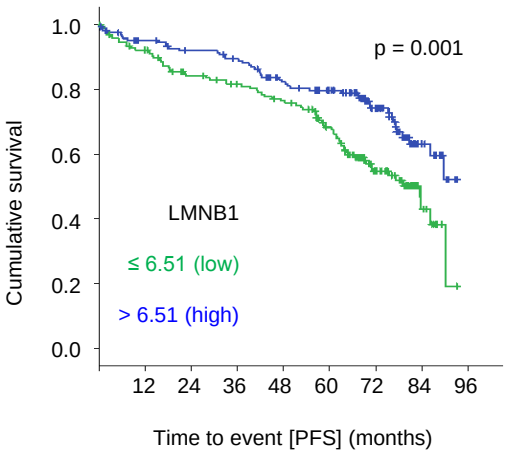
p = 0.001
Cumulative survival
LMNB1
≤ 6.51 (low)
> 6.51 (high)
1.0
0.8
0.6
0.4
0.2
0.0
12 24 36 48 60 72 84 96
Time to event [PFS] (months)

E

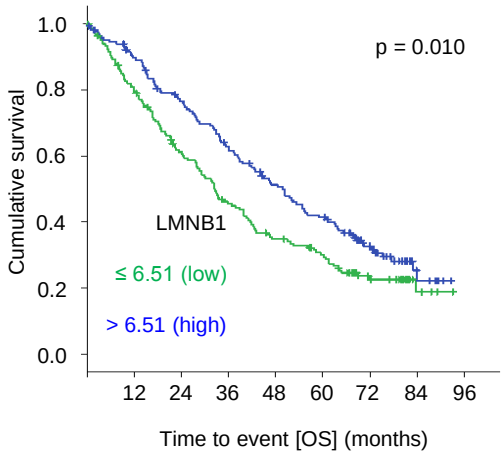
p = 0.010
Cumulative survival
LMNB1
≤ 6.51 (low)
> 6.51 (high)
1.0
0.8
0.6
0.4
0.2
0.0
12 24 36 48 60 72 84 96
Time to event [OS] (months)

F

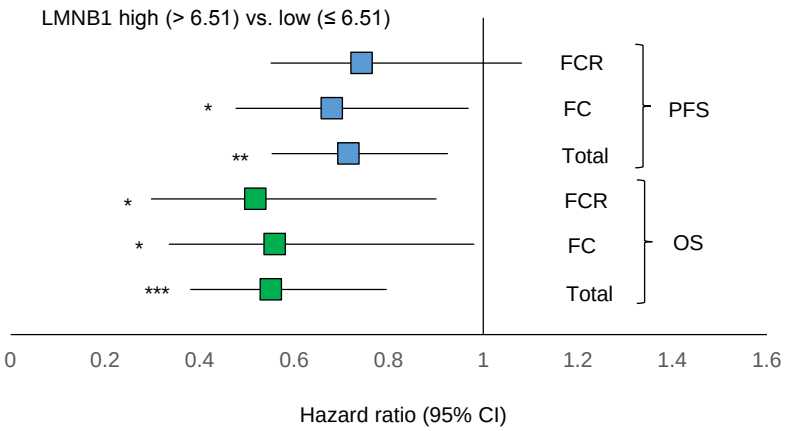
LMNB1 high (> 6.51) vs. low (≤ 6.51)
FCR
FC
Total
PFS
FCR
FC
Total
OS
*
**
*
*
***
0
0.2
0.4
0.6
0.8
1
1.2
1.4
1.6
Hazard ratio (95% CI)

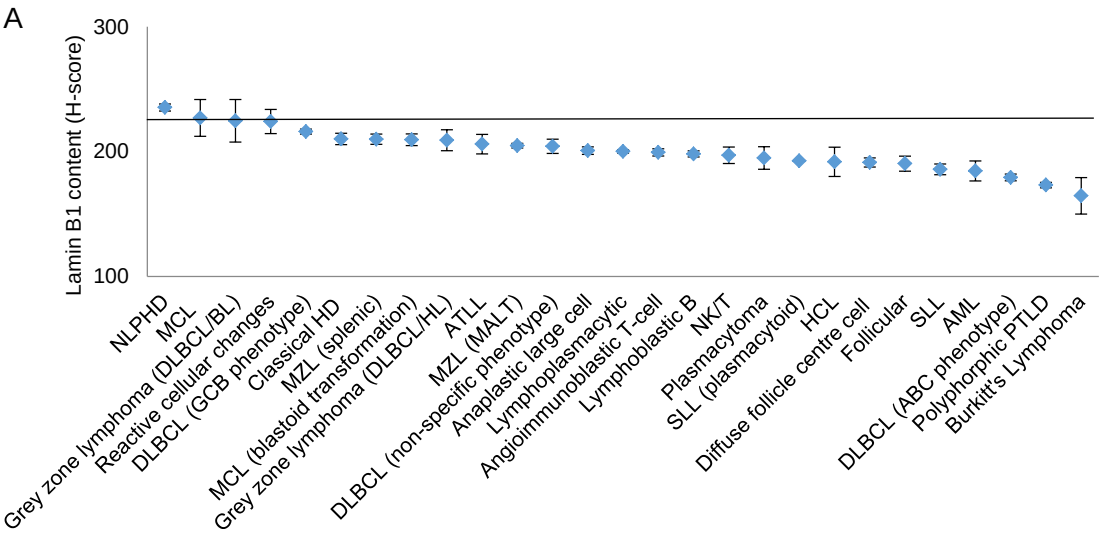
A
Lamin B1 content (H-score)
300
200
100
NLPHD
MCL
Grey zone lymphoma (DLBCL/BL)
Reactive cellular changes
DLBCL (GCB phenotype)
Classical HD
MZL (splenic)
MCL (blastoid transformation)
Grey zone lymphoma (DLBCL/HL)
ATLL
MZL (MALT)
DLBCL (non-specific phenotype)
Anaplastic large cell
Lymphoplasmacytic
Angioimmunoblastic T-cell
Lymphoblastic B
NK/T
Plasmacytoma
SLL (plasmacytoid)
HCL
Diffuse follicle centre cell
Follicular
SLL
AML
DLBCL (ABC phenotype)
Polyphorphic PTLD
Burkitt's Lymphoma

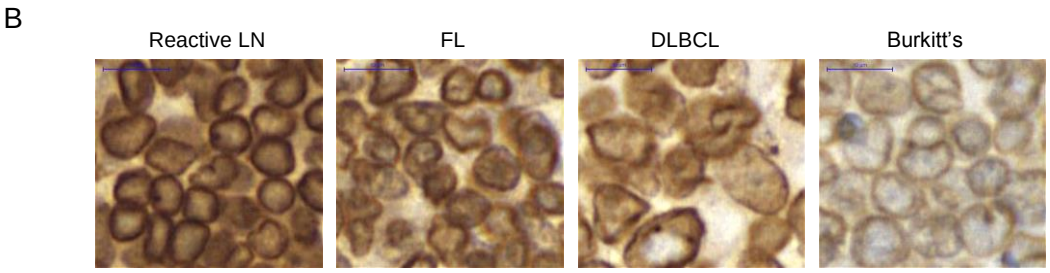
B
Reactive LN
FL
DLBCL
Burkitt's

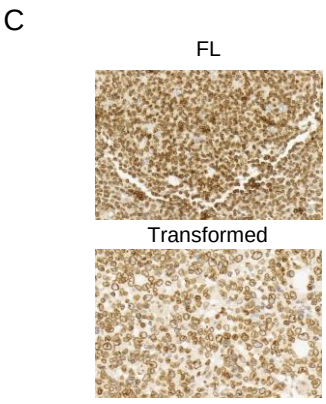
C
FL
Transformed

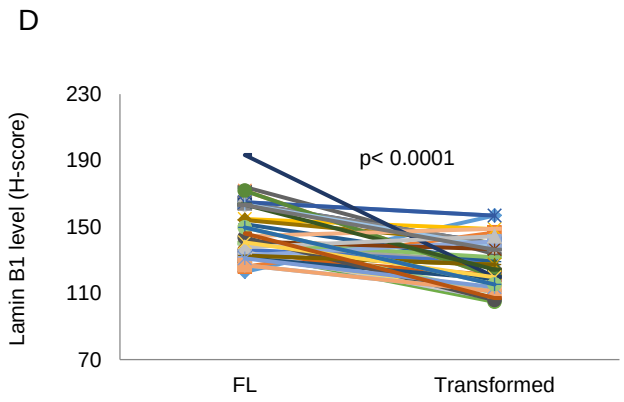
D
Lamin B1 level (H-score)
230
190
150
110
70
p< 0.0001
FL
Transformed

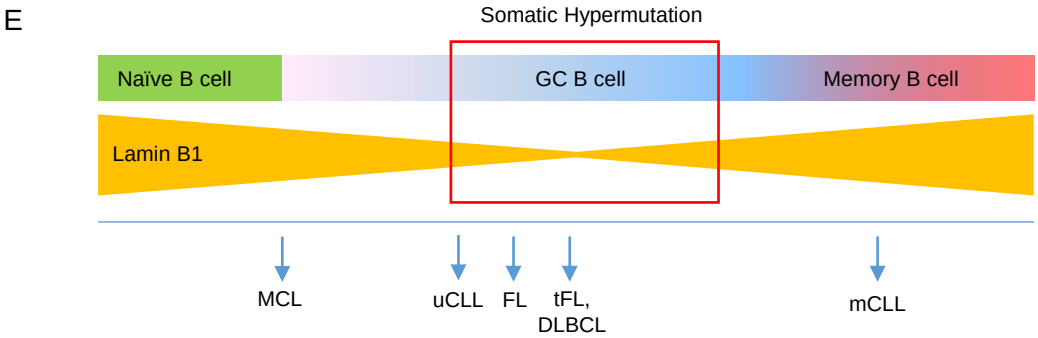
E
Somatic Hypermutation
Naïve B cell
GC B cell
Memory B cell
Lamin B1
MCL
uCLL
FL
tFL, DLBCL
mCLL